# Magnetocaloric properties of rapidly solidified $Dy_3Co$ alloy ribbons

J. L. Sánchez Llamazares, H. Flores-Zúñiga, Pablo Álvarez-Alonso, C. F. Sánchez-Valdés, G. A. Lara Rodríguez, and M. L. Fernández-Gubieda

Citation: Journal of Applied Physics **117**, 17A706 (2015);
View online: https://doi.org/10.1063/1.4906764
View Table of Contents: http://aip.scitation.org/toc/jap/117/17
Published by the American Institute of Physics



# Magnetocaloric properties of rapidly solidified $Dy_3Co$ alloy ribbons

J. L. Sánchez Llamazares,[1,a)] H. Flores-Zúñiga,[1] Pablo Álvarez-Alonso,[2] C. F. Sánchez-Valdés,[1] G. A. Lara Rodríguez,[3] and M. L. Fernández-Gubieda[2,4]
[1]*Instituto Potosino de Investigación Científica y Tecnológica A.C., Camino a la Presa San José 2055 Col. Lomas 4ª, San Luis Potosí, S.L.P. 78216, Mexico*
[2]*Departamento de Electricidad y Electrónica, UPV/EHU, 48940 Leioa, Spain*
[3]*Instituto de Investigaciones en Materiales, Universidad Nacional Autónoma de México, Circuito Exterior s/n, Ciudad Universitaria, México, D. F. 04510, Mexico*
[4]*BC Materials, Camino de Ibaizabal, Edificio 500, Planta 1, Parque Científico y Tecnológico de Zamudio, 48160 Derio, Spain*

(Presented 6 November 2014; received 16 September 2014; accepted 12 October 2014; published online 3 February 2015)

The magnetic and magnetocaloric (MC) properties of melt-spun ribbons of the $Dy_3Co$ intermetallic compound were investigated. Samples were fabricated in an Ar environment using a homemade melt spinner system at a linear speed of the rotating copper wheel of 40 $ms^{-1}$. X-ray diffraction analysis shows that ribbons crystallize into a single-phase with the $Fe_3C$-type orthorhombic crystal structure. The $M(T)$ curve measured at 5 mT reveals the occurrence of a transition at 32 K from a first to a second antiferromagnetic (AFM) state and an AFM-to-paramagnetic transition at $T_N = 43$ K. Furthermore, a metamagnetic transition is observed below $T_N$, but the magnetization change $\Delta M$ is well below the one reported for bulk alloys. Below 12 K, large inverse MC effect and hysteresis losses are observed. This behavior is related to the metamagnetic transition. For a magnetic field change of 5 T (2 T) applied along the ribbon length, the produced ribbons show a peak value of the magnetic entropy change $\Delta S_M^{peak}$ of −6.5 (− 2.1) $Jkg^{-1}K^{-1}$ occurring close to $T_N$ with a full-width at half-maximum $\delta T_{FWHM}$ of 53 (37) K, and refrigerant capacity $RC = 364$ (83) $Jkg^{-1}$ (estimated from the product $|\Delta S_M^{peak}| \times \delta T_{FWHM}$). © *2015 AIP Publishing LLC*.
[http://dx.doi.org/10.1063/1.4906764]

## INTRODUCTION

The development of magnetic refrigeration at cryogenic temperatures demands the assessment of magnetic materials exhibiting a large magnetization change $\Delta M$ through a first- or second-order phase transition.[1] Accordingly, rare-earth (R) based intermetallic compounds are of particular interest due to their large saturation magnetization $M_S$. The R-rich binary $R_3Co$ intermetallic compounds present a large saturation magnetization and different types of first- and second-order magnetic phase transitions in the low-temperature range.[2–4] Among them, the compound $Dy_3Co$, which crystallizes into the orthorhombic $Fe_3C$-type crystal structure (space group Pnma),[5] exhibits a complex antiferromagnetic (AFM) behavior with different non-collinear AFM structures below its Néel temperature $T_N = 44$ K.[6,7] Its magnetic phase diagram can be consulted in Refs. 6 and 8. Furthermore, magnetic-field-induced transitions have been observed along the three main crystallographic axes;[6–8] in particular, this occurs along the $c$ axis for an applied magnetic field $\mu_o H$ below 2 T and gives rise to a large $\Delta M$. For obtaining a large magnetocaloric (MC) effect, this is a favorable condition. In fact, Shen *et al.* have recently studied the MC properties of bulk polycrystalline alloys of this intermetallic phase produced after a prolonged thermal homogenization annealing at 873 K (8 days);[9] they found large values of the maximum magnetic entropy change $\Delta S_M^{peak}$ and refrigerant capacity $RC$ (−13.9 $Jkg^{-1}K^{-1}$ and 498 $Jkg^{-1}$, respectively, for $\mu_o \Delta H = 5$ T).

As far as we know, the only previous work on the fabrication of melt-spun $Dy_3Co$ ribbons is that of Baranov *et al.*[10] These authors refer the synthesis by this technique of amorphous $R_3Co$ ribbons with R = Nd, Tb, and Dy, and present a preliminary magnetic characterization (i.e., the temperature dependence of both the AC magnetic susceptibility and hysteresis loops). They highlight that, in contrast with the reported for crystalline samples, the magnetic structure of amorphous $Dy_3Co$ is asperomagnetic below an ordering temperature of 38 K. In addition, below 14 K the coercive field $\mu_o H_C$ rises as temperature decreases to reach a value of around 1 T at 2 K. However, neither the processing conditions used to fabricate the ribbons nor their characterization by X-ray diffraction (XRD) were reported.

This investigation was undertaken to produce melt-spun polycrystalline ribbons of the $Dy_3Co$ intermetallic compound in order to assess the magnetic and MC properties. It must be emphasized that this processing technique has been recently applied to fabricate ribbon samples of several rare-earth based magnetocaloric alloys, such as $RNi_2$ with R = Tb or Dy,[11,12] and $NdPrFe_{17}$[13] with positive results: (a) the processing conditions are improved since a prolonged thermal annealing is not necessary in order to produce a single-phase material; (b) in some alloys, such as $DyNi_2$ and $NdPrFe_{17}$, a considerable enhancement of the refrigerant capacity $RC$ has been observed

a)Author to whom correspondence should be addressed. Electronic mail: jose.sanchez@ipicyt.edu.mx.

 

in comparison with that reported for their bulk counterpart alloys.

## EXPERIMENTAL PROCEDURE

As-quenched alloy ribbons of ~15–18 $\mu$m thick [see the inset of Fig. 1(a), where the typical cross-section of ribbons is shown], with 1.5–2.0 mm in width and 7–10 cm in length, were fabricated from argon arc-melted as-cast bulk ingots previously produced from highly pure elements (99.98% pure Co and 99.9% pure Dy). The molten induction melted alloy was ejected through a circular nozzle of 0.5 mm onto the polished surface of a rotating copper wheel at a linear speed of 40 $ms^{-1}$. The process was carried out in a highly pure argon environment. Microstructure and elemental composition were determined using a FEI/Philips XL30 FEG ESEM equipped with an energy dispersive analysis system (EDS). Room temperature XRD patterns for ribbon samples were obtained with a Bruker AXS model D8 Advance diffractometer (Cu-K$\alpha$ radiation; scanning interval: $20° \leq 2\theta \leq 80°$; step increment: 0.02°). Le Bail analysis of the diffraction patterns for ribbons and finely powdered ribbons was carried out through the FullProf Suite.[14]

Magnetization measurements were performed on ribbon samples using a Quantum Design PPMS® EverCool-I 9 T platform. The magnetic field $\mu_o H$ was applied along the ribbon axis (rolling direction) to minimize the demagnetizing field effect. The magnetization as a function of temperature $M(T)$ curve was recorded on heating at 1.5 K/min under $\mu_o H = 10$ mT. The Néel temperature $T_N$ of the higher temperature magnetic sublattice was obtained by extrapolation to the $T$ axis of the thermal dependence of the reciprocal magnetic susceptibility ($1/\chi$). The magnetic entropy change as a function of temperature $\Delta S_M(T)$ was obtained by numerical integration of the Maxwell relation from a set of isothermal magnetization curves $M(\mu_o H)$ measured from 3 to 126 K, up to a maximum applied magnetic field of $\mu_o H = 5$ T [shown in Fig. 2(a)]. Due to the complex antiferromagnetic order of the $Dy_3Co$ compound and the occurrence of a first-order field-induced phase transition, the thermal protocol chosen to measure the isothermal magnetization curves below $T_N$ ensured that the phase transition is always crossed in the same direction (i.e., from a lower to higher temperature). The latter allowed a correct determination of the $\Delta S_M(T)$ as well as the evaluation of hysteresis losses associated to the irreversibility of the $M(\mu_o H)$ curves.

The refrigerant capacity $RC$ was estimated from the $\Delta S_M(T)$ curves. The definition of $RC$–1, $RC$-2, and $RC$–3 can be found in Ref. 15. The magnetic hysteresis losses were estimated from the area between the virgin and demagnetizing $M(\mu_o H)$ curves in the first quadrant measured at different temperatures below $T_N$.[16]

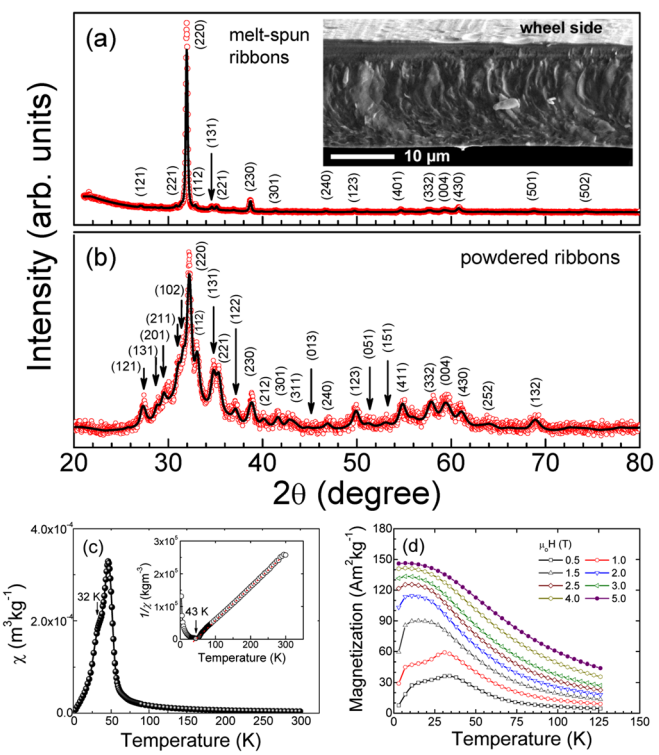


FIG. 1. Room temperature X-ray diffraction pattern measured for as-solidified (a) and manually powdered (b) $Dy_3Co$ ribbons. Inset in (a): typical SEM micrograph of the typical cross-section microstructure for the fabricated ribbon samples. (c) Thermal dependence of the magnetic susceptibility $\chi(T)$ measured at 10 mT for as-solidified $Dy_3Co$ ribbons. The inset shows the thermal dependence of the reciprocal susceptibility. A Néel temperature of 43 K was estimated from the extrapolation in the paramagnetic region. (d) $M(T)$ curves for increasing selected magnetic field values.

## RESULTS AND DISCUSSION

The EDS analysis (not shown) performed on the ribbons revealed that the chemical composition of as-solidified ribbons coincides with the nominal one, i.e., $Dy_3Co$, within the experimental error (typically 0.1 at. %). The diffraction peaks in the X-ray diffraction pattern, shown in Fig. 1(a), can be indexed

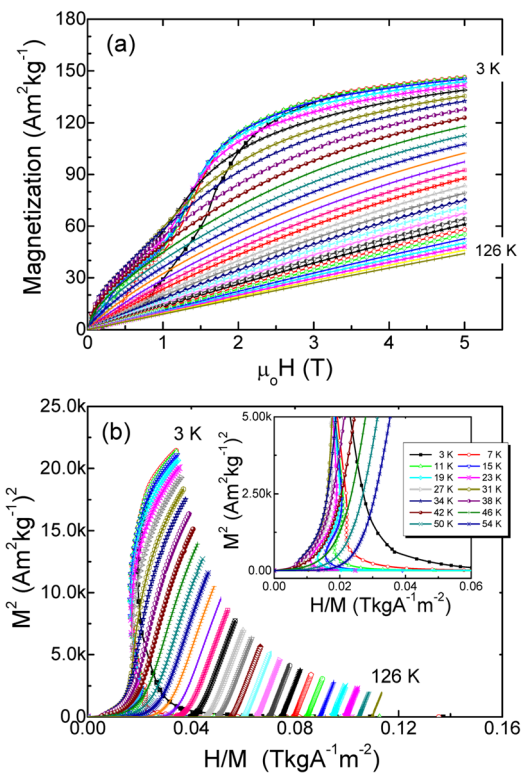


FIG. 2. Isothermal magnetization curves measured from 3 to 126 K for as-quenched $Dy_3Co$ ribbons (a) and the corresponding Arrott plots (b).

assuming a $Fe_3C$-type crystal structure (space group Pnma) with the cell parameters $a = 6.9646(8)$ Å, $b = 9.345(1)$ Å, and $c = 6.2238(7)$ Å (cell volume, $V = 405.07(9)$ Å$^3$). No traces of a different phase, either amorphous or crystalline, have been observed. This is in apparent contradiction with the reported in Ref. 10, where the authors claimed that ribbons are amorphous, and is probably due to the different fabrication conditions.

As the relative intensity between several Bragg diffraction peaks clearly indicates the existence of texture, we manually powdered some ribbons and measured the XRD pattern [see Fig. 1(b)]. The existence of a large preferential orientation along the (220) direction for the ribbons is clearly shown [compare Figs. 1(a) and 1(b)]. This should be related with a preferential growth of grains and it is well-known that is a characteristic feature of many materials produced by this technique related to the temperature gradient during solidification.[10] Furthermore, we noted that the powdering process induces a widening of the diffraction peaks mainly due to the reduction of crystalline size. However, it must be noticed that the cell parameters do not differ significantly from those of the bulk.[6]

The extrapolation of the inverse of the susceptibility $1/\chi(T)$ [see the inset of Fig. 1(c)] shows the presence of a second-order AFM-to-paramagnetic (PM) transition at $43.0 \pm 0.5$ K (indicated by the vertical arrow). However, the presence of a shoulder in the $\chi(T)$ curve at $32.0 \pm 0.5$ K indicates an additional magnetic phase transition that, in the bulk material, has been associated to a change in the magnetic ordering from two different AFM states (i.e., AFM-1 to AFM-2).[6,8] The isothermal magnetization curves $M(\mu_oH)$ are plotted in Fig. 2(a); as expected from the magnetic susceptibility measurements, the $M(\mu_oH)$ curves exhibit a paramagnetic behavior above the Néel temperature; below $T_N$, the magnetization depends linearly with the applied magnetic field in the low field range, but at a certain critical magnetic field ($\sim$ 1T) increases steeply, indicating the occurrence of a magnetic-field induced transition (it is interesting to note that $M$ value obtained at 5 T is close to the reported value in Ref. 8). Accordingly, the curves of the temperature dependence of the magnetization of the ribbons [depicted in Fig. 1(d)] for fields over 3 T correspond to a ferromagnetic metastable state, whereas for lower fields the magnetization shows two peaks at the AFM-1 to AFM-2 and AFM-2 to PM magnetic phase transitions, as occurs in the polycrystalline $Dy_3Co$ bulk alloy.[9] To ascertain the first-order character of the metamagnetic transition, in Fig. 2(b) we have represented the Arrott plots; we noted that those isothermal curves below $T_N$ show a $S$-shape, which—according to the Banjeree's criteria[17]—confirms the first-order character for the AFM-to-FM induced magnetic phase transition. Above $T_N$, the Arrott plots are concave upward with a positive slope indicating the second-order character of the FM-to-PM transition.

Figure 3(a) shows the $\Delta S_M(T)$ curves measured for different applied magnetic field changes. The magnetic entropy shows large positive values below 12 K. It is worth noting that the measurements have been performed considering the metamagnetic transition. Furthermore, the curve at $\mu_o\Delta H = 1$ T presents positive values at temperatures below $T_N$ that decreases with increasing magnetic field, and eventually become negative. A similar behavior has been ascribed to the magnetic-field induced phase transition by Shen and coworkers.[9] The minimum of the curves reaches close to $T = T_N$ ($\sim$ 40 K) due to the FM-to-PM phase transition at large fields. However, the magnetic field dependence of $|\Delta S_M{}^{peak}|$ [plotted in the left inset of Fig. 3(a)] follows a $(\mu_o\Delta H)^n$ law with $n > 1$ for magnetic field changes below 2 T, but $n$ tends to $\sim$1 for higher magnetic fields; this change in the exponent close to the critical field of the metamagnetic transition indicates that it affects the magnetic field dependence of $\Delta S_M(T)$. Table I summarizes the main MC properties of the polycrystalline ribbons and compares them with that which was obtained in bulk alloys.[9] One can observe that the value of $|\Delta S_M{}^{peak}|$ at $\mu_o\Delta H = 5$ T for the bulk alloy is almost twice than in ribbons. The reason for that is twofold. On the one hand, the $Dy_3Co$ ribbons present smother magnetic transitions—as generally occurs in ribbons with a magnetic transition distribution[13,18]—which are accompanied by an enlargement of the width of the

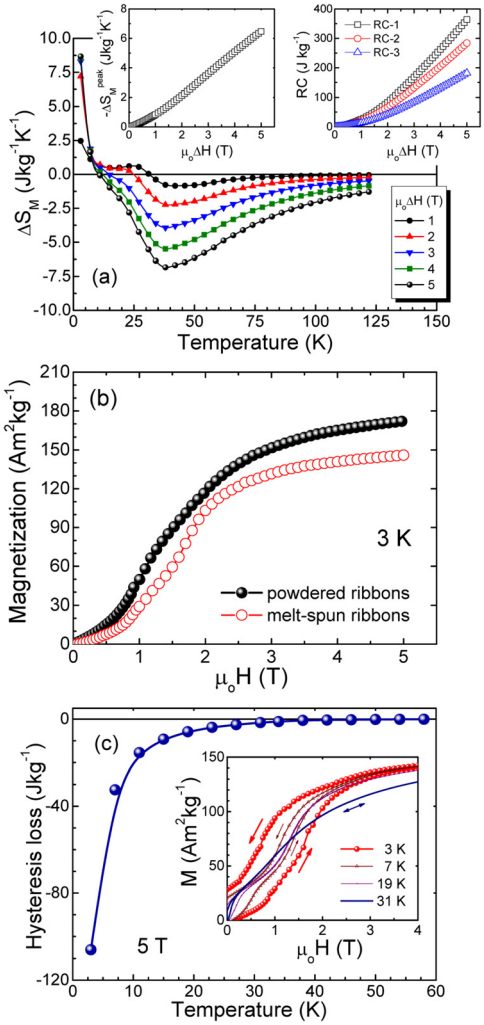


FIG. 3. (a) $\Delta S_M(T)$ curves for magnetic field change values $\mu_o\Delta H$ from 1 to 5 T. Left inset: $|\Delta S_M|^{peak}$ versus $\mu_o\Delta H$. Right inset: Refrigerant capacities $RC$-1, $RC$-2, and $RC$-3 as a function of $\mu_o\Delta H$. (b) Comparison of the magnetization isotherm measured at 3 K for as-solidified and manually powdered ribbons. (c) Thermal dependence of the hysteresis losses measured for a field change of 5 T below 40 K. Inset: magnetization isotherms for increasing and decreasing the magnetic field (as indicated by the arrows) at selected temperature values to illustrate the origin of hysteresis losses shown by the material.

TABLE I. Peak magnetic entropy change $|\Delta S_M{}^{peak}|$, *RC*-1, *RC*-2, $\delta T_{FWHM}$, $T_{hot}$, $T_{cold}$, *RC*-3, $\delta T^{RC\text{-}3}$, and $T_{hot}{}^{RC\text{-}3}$ and $T_{cold}{}^{RC\text{-}3}$ related to *RC*-3 for $Dy_3Co$ ribbons. All of them are given for magnetic field changes $\mu_o\Delta H$ of 2 and 5 T. For the sake of comparison, the magnetocaloric properties recently reported by Shen *et al.*[9] for bulk alloys are listed.

| | $Dy_3Co$ ribbons $\mu_o\Delta H$ (T) | | $Dy_3Co$ bulk $\mu_o\Delta H$ (T) | |
|---|---|---|---|---|
| | 2 T | 5 T | 2 T | 5 T |
| $\lvert\Delta S_M{}^{peak}\rvert$ (J kg$^{-1}$ K$^{-1}$) | 2.1 | 6.5 | 5.0 | 13.9 |
| *RC*-1 (J kg$^{-1}$) | 83 | 364 | … | 614[b] |
| *RC*-2 (J kg$^{-1}$) | 67 | 284 | … | 498 |
| $\delta T_{FWHM}$ (K) | 37 | 53 | … | 45 |
| $T_{hot}$ (K) | 67 | 78 | … | 68 |
| $T_{cold}$ (K) | 30 | 25 | … | 23 |
| *RC*-3 (J kg$^{-1}$) | 42 | 182 | … | 310[b] |
| $\delta T^{RC\text{-}3}$ (K)[a] | 33 | 53 | … | 47[b] |
| $T_{hot}{}^{RC\text{-}3}$ (K)[a] | 64 | 78 | … | 70[b] |
| $T_{cold}{}^{RC\text{-}3}$ (K)[a] | 31 | 25 | … | 23[b] |

[a]Related to *RC*-3.
[b]Estimated from the $\Delta S_M$(T) curve reported Ref. 9.

curve that, unlike other cases, here it does not lead to an enhancement of the refrigerant capacity. The reader must note that the broadening of the $\Delta S_M(T)$ curve, compared to that of the bulk, hides the effect of the AFM-1 to AFM-2 phase transition, as this transition has associated a clear peak in the bulk but not in the ribbons. On the other hand, the XRD pattern provides clear evidence on ribbons texture. Thus, the magnetization reduction could be due to a relatively large volume fraction of grains are oriented with their crystallographic direction [110] along ribbon length. As this hard magnetization axis is parallel to the applied magnetic field, the magnetization would become lower than for other directions thus reducing the maximum magnetic entropy change. In order to prove this hypothesis in Fig. 3(b), we compare the isothermal magnetization curve measured at 3 K for both melt-spun ribbons and a cylindrical in shape sample made from manually powdered ribbons; the $\mu_oH$ axis of the M($\mu_oH$) curve for this powder sample with most of grains randomly oriented was corrected due to the demagnetizing field effect. It is clearly seen that the magnetization at 5 T for the powdered sample (172 Am$^2$kg$^{-1}$) is a 17.8% higher than that measured for the as-solidified ribbons (146 Am$^2$kg$^{-1}$), indicating that in the fabricated ribbons crystallographic texture diminishes $\lvert\Delta S_M{}^{peak}\rvert$ when the magnetic field is applied along the ribbon length.

To make more complete our analysis, we estimated the magnetic hysteresis losses from the increasing-decreasing magnetic field dependence of the magnetization [see their typical shape at the inset of Fig. 3(c) for four representative temperatures below $T_N$]. Clearly, losses for $\mu_o\Delta H = 5$ T, whose temperature dependence is shown in Fig. 3(c), increase as the temperature decreases reaching a large value of 105 Jkg$^{-1}$ at 3 K. They occur at those temperatures, where the magnetic field-induced transition takes place [see Fig. 3(c)]. The *RC* values summarized in Table I are given (the hysteresis losses were not subtracted), while their dependence on $\mu_o\Delta H$ is given in the right inset of Fig. 3(a).

## CONCLUSIONS

We have synthesized the polycrystalline $Dy_3Co$ alloy in ribbon shape using the melt-spinning technique at a high linear wheel speed of 40 ms$^{-1}$. The ribbons show an AFM-1 to AFM-2 phase transition at $32.0 \pm 0.5$ K followed by an AFM-2 to PM at $T_N \approx 43.0$ K. The positive values of the magnetic entropy change are associated to the AFM state, whereas the magnetic field-induced phase transition from an AFM phase to the FM state is the responsible of the continuous decrease of the magnetic entropy change. The maximum absolute value of the magnetic entropy change (6.5 Jkg$^{-1}$K$^{-1}$ at $\mu_o\Delta H = 5$ T) occurs close to the Néel temperature; the $\lvert\Delta S_M{}^{peak}\rvert$ values of the ribbons for $\mu_o\Delta H = 2$ and 5 T are low in comparison with those reported for the bulk alloys, as a direct consequence of both the lower values of the magnetization change due to the metamagnetic transition and the broader $M(T)$ dependence.

## ACKNOWLEDGMENTS

Authors acknowledge: (a) the financial support received from Grant CB-2010-01-156932 (CONACyT, Mexico), and Laboratorio Nacional de Investigaciones en Nanociencias y Nanotecnología (LINAN, IPICYT), (b) the technical support received from Dr. G. J. Labrada-Delgado and M.Sc. B. A. Rivera Escoto during SEM observations and XRD diffraction experiments, respectively. C. F. Sánchez-Valdés is grateful to LINAN, IPICyT, and CONACyT (Project No. CB-2012-01-183770) for supporting his postdoctoral stay.

[1]K. A. Gschneidner, Jr., V. Pecharsky, and A. O. Tsokol, Rep. Prog. Phys. **68**, 1479 (2005).
[2]G. J. Primavesi and K. N. R. Taylor, J. Phys. F: Met. Phys. **2**, 761 (1972).
[3]K. Sato, I. Umehara, N. Fujimori, M. Hamano, K. Nakano, T. Fukuhara, and K. Maezawa, Physica B **199–200**, 651 (1994).
[4]N. V. Tristan, K. Nenkov, T. Palewski, K. P. Skokov, and S. A. Nikitin, Phys. Status Solidi A **196**, 325 (2003).
[5]K. H. J. Buschow, Rep. Prog. Phys. **40**, 1179 (1977).
[6]N. V. Baranov, A. N. Pirogov, and A. E. Teplykh, J. Alloys Compd. **226**, 70 (1995).
[7]N. V. Baranov, E. Bauer, R. Hauser, A. Galatanu, Y. Aoki, and H. Sato, Eur. Phys. J. B **16**, 67 (2000).
[8]P. Svoboda, H. Nakotte, A. Alsmadi, and M. Doerr, Acta Phys. Pol. B **34**, 1449 (2003).
[9]J. Shen, J. L. Zhao, F. X. Hu, G. H. Rao, G. Y. Liu, J. F. Wu, Y. X. Li, J. R. Sun, and B. G. Shen, Appl. Phys. A **99**, 853 (2010).
[10]N. V. Baranov, V. I. Pushkarski, A. E. Sviderski, and H. Sassik, J. Magn. Magn. Mater. **157–158**, 635 (1996).
[11]J. L. Sánchez Llamazares, C. F. Sánchez-Valdés, P. J. Ibarra-Gaytan, P. Álvarez-Alonso, P. Gorria, and J. A. Blanco, J. Appl. Phys. **113**, 17A912 (2013).
[12]P. J. Ibarra-Gaytan, C. F. Sánchez-Valdés, J. L. Sánchez Llamazares, P. Álvarez-Alonso, P. Gorria, and J. A. Blanco, Appl. Phys. Lett. **103**, 152401 (2013).
[13]C. F. Sánchez-Valdés, P. J. Ibarra-Gaytán, J. L. Sánchez Llamazares, M. Ávalos-Borja, P. Álvarez-Alonso, P. Gorria, and J. A. Blanco, Appl. Phys. Lett. **104**, 212401 (2014).
[14]J. Rodríguez-Carvajal, Phys. B Condens. Matter **192**, 55 (1993).
[15]P. Gorria, J. L. Sánchez Llamazares, P. Álvarez, M. J. Pérez, J. Sánchez Marcos, and J. A. Blanco, J. Phys. D: Appl. Phys. **41**, 192003 (2008).
[16]V. Provenzano, A. J. Shapiro, and R. D. Shull, Nature **429**, 853 (2004).
[17]B. K. Banerjee, Phys. Lett. **12**, 16 (1964).
[18]G. Daniel-Pérez, J. L. Sánchez Llamazares, A. Quintana-Nedelcos, P. Álvarez-Alonso, R. Varga, and V. Chernenko, J. Appl. Phys. **115**, 17A920 (2014).